Real-Time Multi-Sensor-Based Data Acquisition System for Industrial Safety Monitoring

Sahil Dhown

https://orcid.org/0009-0000-7509-6228

***Abstract* - Monitoring machinery is vital for detecting faults at an early stage before any hazardous incident occurs. A defect warning on the screen appears when vibration exceeds 6.5 meters per second squared due to an invisible bearing defect in machinery. Additionally, temperature sensors can detect overheating over time under these conditions. Otherwise, it remains normal and at a safe level based on the local visualization. This paper presents the development of a project and outlines the methods, including a design, tests, and equations used. Despite having multiple sensors affecting the performance speed, the system has satisfied real-time monitoring criteria, delivering the response of each output result within less than 35 milliseconds (0.035 s). This real-time data-acquisition-based electronic prototype closely aligns with industry standard principles and successfully recognizes both normal and faulty operations in industrial machinery. This 3-channel STM32-based project cut costs by 98% compared to a traditional and expensive 3-channel vibration monitoring device, helping corporations save costs and improve operator safety.**

***KEYWORDS*:** Sensors; Hardware prototype; Industrial monitoring; STM32; Vibration analysis; Charge amplification; RMS acceleration; Data acquisition system; Machinery; Industry standards; Frequency; Real-time performance; Defect diagnosis.

I. INTRODUCTION

Industrial monitoring plays a critical role in reducing high maintenance overheads and mitigating hazardous workplace risks by avoiding sudden equipment breakdowns [1]. The increasing use of piezoelectric disc sensors in new industrial applications, including the aerospace and medical sectors, demonstrates their potential for future growth, as they provide advantages such as miniaturization for compact devices and high sensitivity to acceleration [2]. Real-time vibration acquisition using an STM32 microcontroller, which is also widely used for industrial purposes, can predict and diagnose machinery conditions by analyzing sensor-detected vibration data. This improves economic efficiency and minimizes maintenance time. The STM32 platform is an essential part of the defect diagnosis system and leverages ARM technology for embedded systems to support real-time performance, large data capacity, portability, and miniaturization [3]. This functional prototype project is composed of a data acquisition system within the microcontroller (STM23) running HAL-based code in C, charge amplification involving a TL081 due to its high slew rate of between 13-16 V/μs based on the datasheet (as shown in the table of the BOM), a high-pass filter (a low-cut filter), the power supply, and multiple sensors, including industrial temperature sensors, as well as piezoelectric disc sensors that capture physical vibrations for measurements in Hertz and ms^{-2}. The high-speed STM32 microcontroller, with a 72 MHz clock, was programmed using the sophisticated software called STM32CubeIDE. This paper presents a circuit analysis of charge amplification and a set of mathematical equations, including low- and high-cut frequencies, resistive gain and capacitive gain, the zero-crossing rate of the frequency signal, and RMS acceleration using RMS voltage and sensitivity, which are applied to measure vibration. In addition, the equation for the average heating rate is calculated after scaling the temperature. This work also indicates how verification of the physical project's functional performance was conducted and how the output display was assessed to distinguish faulty performance from normal operation in machinery based on the guidelines of an industry standard.

II. METHODOLOGY

A. BLOCK DIAGRAM OF A DATA ACQUISITION SYSTEM WITH SENSORS

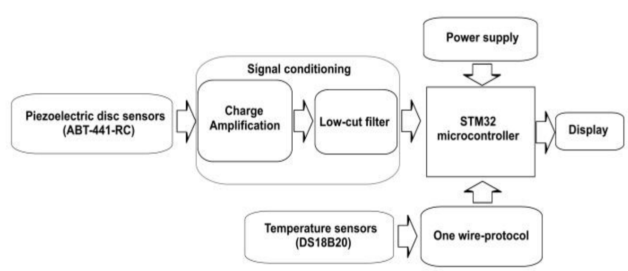

Figure 1. Block diagram of a data acquisition system for industrial safety monitoring.

Based on the block diagram in Figure 1, the 32-bit STM32 microcontroller performs real-time data acquisition when the multi-sensors, including piezoelectric disc sensors and DS18B20 sensors, emit

https://orcid.org/0009-0000-7509-6228

analog and digital signals via signal conditioning (involving the charge amplification and a low-cut filter) and the one-wire protocol, respectively, both connecting to the µC. It is actually a 3-channel prototype, with each channel carrying two sensors (vibration and temperature). The detected signals are processed by the microcontroller and displayed on the screen. For example, when the display shows a defect sign due to abnormal bearing operation, it helps reduce maintenance time and effort.

B. AN ENTIRE SCHEMATIC CIRCUIT OF A DATA ACQUISITION SYSTEM WITH MULTIPLE SENSORS

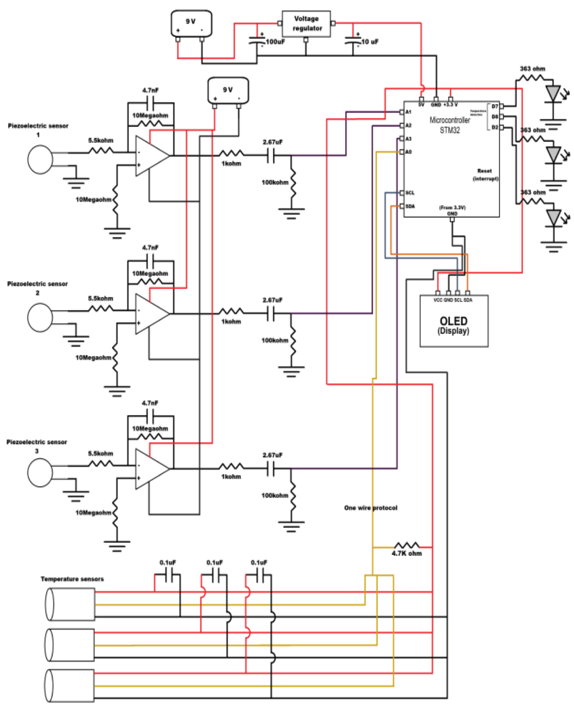

Figure 2. A schematic circuit diagram of a data acquisition system for industrial safety monitoring.

This section details the functions of industrial monitoring functions, the integration of circuit components, and their communication with the µC to run operations simultaneously. In Figure 2, when a mechanical force acts on the piezoelectric disc sensor, it generates a weak and raw electrical signal that can be amplified into a readable signal after entering the charge-amplification circuit, which is derived from [4], with the feedback components (4.7 nF and 10 MΩ). Another 10 MΩ resistor is placed between the non-inverting terminal of an operational amplifier and ground to prevent output error. Once the amplified output signals from the filtering circuits are received, they are individually fed into the µC via the analog input pins (A1 or ADC channel 1, A2 or ADC channel 4, and A3 or ADC channel 8). Meanwhile, each decoupling capacitor (0.1 µF) connects between VDD (3.3 V) and ground on each digital temperature sensor, maintaining a stable signal transmission. The one-wire protocol, as in the yellow wire, carries the detected signals in binary form through a single pin (A0), with a 4.7 kΩ pull-up resistor connected to VDD. The OLED connects to the high-frequency STM32 via the I2C interface and displays the output on the screen based on the multi-sensor readings of the condition.

C. A CIRCUIT ANALYSIS AND SIMULATION OF THE CHARGE AMPLIFICATION

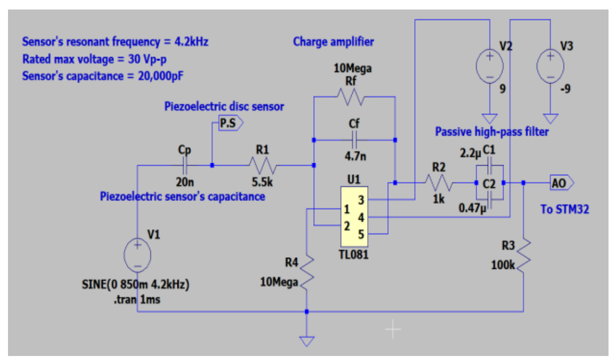

Figure 3. Using LTspice to simulate the charge amplification circuit with a low-cut filter for an output. Based on the datasheet of a 27 mm piezoelectric disc sensor shown in the table of the BOM, the piezoelectric sensor's capacitance is 20,000 pF and the resonant frequency is 4.2 kHz.

- The resistive gain and capacitive gain from the charge amplifier, as shown in Figure 3, are being evaluated using external components. For the resistive gain, it is the ratio of the feedback resistance (R_f) and series resistance (R_1) with a minus sign. For the capacitive gain, it is the ratio of the piezoelectric disc sensor's capacitance (C_p) and the feedback capacitance (C_f) with a minus sign. Both resistive gain and capacitive gain require careful balance using the right value of external components in order to ensure that this circuit amplifies a weak signal from a piezoelectric disc sensor into a measurable signal for the STM32 microcontroller to read clearly. Such calculations can be expressed below

$$\text{Resistive gain} = -\frac{\text{feedback resistance}}{\text{series resistance}}$$

$$\text{Resistive gain} = -\frac{-10\ \text{MegaOhm}}{5.5\ \text{kOhm}} = -1818 \qquad (1)$$

$$\text{Capacitive gain} = -\frac{\text{sensor's capacitance}}{\text{feedback capacitance}}$$

$$\text{Capacitive gain} = -\frac{20\text{nF}}{4.7\text{nF}} = -\frac{20{,}000\text{pF}}{4{,}700\text{pF}} = -4.254 \qquad (2)$$

- The application of the cut-off frequency formula, derived from [4], to circuit analysis is shown below

$$f_c = \frac{1}{2\pi RC}$$

Where f_c is the cut – off frequency,
R is the resistance and C is the capacitance.

- The input circuit before the charge amplifier is analyzed using an upper cut-off frequency (low-pass filter) with the series resistance (R_1) and the piezoelectric disc sensor's capacitance (C_p). It provides a low-pass filter effect. The calculation of a cut-off frequency for an input circuit can be expressed below

$$f_c\ (\text{input circuit}) = \frac{1}{2\pi R_1 C_p}$$

$$= \frac{1}{2 \text{ x } 3.14 \text{ x } 5.5\text{k}\Omega \text{ x } 20\text{nF}}$$

$$= \frac{1}{2 \text{ x } 3.14 \text{ x } 5500 \text{ x } 2 \text{ x } 10^{-8}}$$

$$= 1447.59 \text{ Hz} \qquad (3)$$

- The feedback circuit across the charge amplifier is analyzed using a cutoff frequency with feedback resistance (R_f) and feedback capacitance (C_f). The feedback components of the charge amplifier are determined by

$$f_c(\text{across charge amplifier}) = \frac{1}{2\pi R_f C_f}$$

$$= \frac{1}{2 \text{ x } 3.14 \text{ x } 10 \text{ Megaohm x } 4.7\text{nF}}$$

$$= \frac{1}{2 \text{ x } 3.14 \text{ x } 10{,}000{,}000 \text{ x } 4.7 \text{ x } 10^{-9}} = 3.38799 \text{ Hz} \qquad (4)$$

- The passive high-pass filter is placed on the circuit after the charge amplifier and involves the capacitors ($C_1$and C_2) and the resistor (R_3) that is connected to the ground. It has the ability to filter out unwanted low-frequency noise. The calculation is shown below

$$f_c = \frac{1}{2\pi R_3(C_1 + C_2)}$$

$$= \frac{1}{2 \text{ x } 3.14 \text{ x } 100{,}000 \text{ Ohm x } 2.67\ \mu\text{F}}$$

$$= \frac{1}{2 \text{ x } 3.14 \text{ x } 100{,}000 \text{ x } 2.67 \text{ x } 10^{-6}}$$

$$= \frac{1}{1.67676} = 5.96 \text{ x } 10^{-1} = 0.596 \text{ Hz} \qquad (5)$$

- The sensitivity of the piezoelectric disc sensor with the charge amplifier can be evaluated using the electrical charge (Q) stored in the feedback capacitance (C_f), as shown below

$$Q = (-V_{out})C_f$$

$$V_{out} = -\frac{Q}{C_f} = \text{sensitivity}$$

The charge (Q) as a piezoelectric charge coefficient in the longitudinal mode for a soft PZT (high sensitivity to vibration) is typically around 400 pC/N, which falls within the typical range of 300- 600 pC/N [2],[5].

$$\text{Sensitivity} = -\frac{400 \text{ pC/N}}{4700 \text{ pF}}$$

$$= -\frac{400 \text{ pC/N}}{4700 \text{ pC/V}} \quad [\text{pF} = \text{pC/V}]$$

$$\text{Sensitivity} = -8.51063 \text{ x } 10^{-2} \text{ V/N}$$

$$\text{Sensitivity} = +8.51063 \text{ x } 10^{-2} \text{ V/N} \qquad (6)$$

As the minus sign is neglected for the calculation of acceleration in ms^{-2} on the next page.

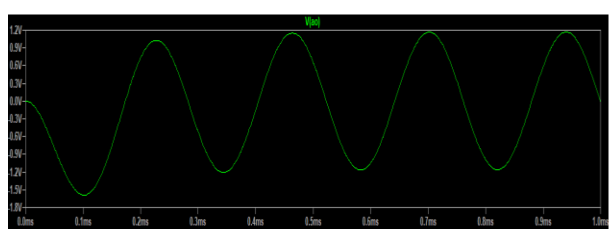

Figure 4. The simulation result was successfully obtained after

https://orcid.org/0009-0000-7509-6228

applying an input voltage of 850mV from a piezoelectric sensor through the circuit (see Figure 3).

D. TESTED A CIRCUIT DESIGN OF THE CHARGE AMPLIFICATION ON A BREADBOARD FOR PRACTICAL VERIFICATION

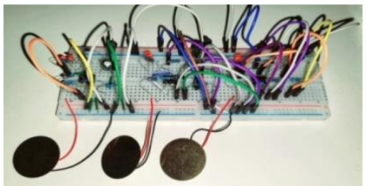

Figure 5. Tested the circuits on a breadboard with three piezoelectric disc sensors.

A physical circuit was being built and tested to ensure that it matched the behaviour of the simulation in LTspice (see Figure 4). After testing with minimal and high mechanical motion on each sensor, the digital multimeter readings ranged from 0.8V to 3.36V. This range is well-suited and safe for the STM32's 3.3 V (maximum voltage value) input pins. The breadboard in Figure 5 was filled with electronic components, including resistors, capacitors, and operational amplifiers, as well as piezoelectric disc sensors, all connected by numerous jumper wires. They operated only when the battery (9V) was connected and were practically verified before the assembly of a dotted PCB.

E. INCREASING THE SAMPLING RATE OF A DIGITIZED ANALOG SIGNAL TO PREVENT ALIASING EFFECT

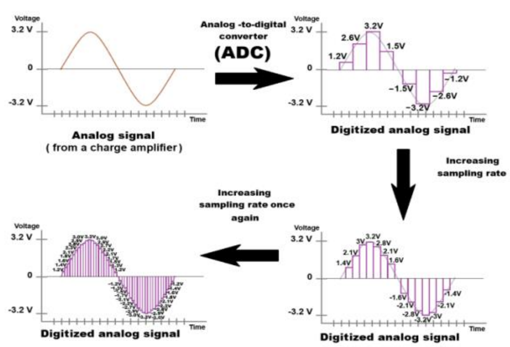

Figure 6. After switching the clock from 8MHz to 72MHz in the STM32CubeIDE settings, a dense digitized analog signal is achieved by manually decreasing the sampling time while allowing the sampling rate to increase.

The sampling frequency (f_s) should be higher than twice the maximum frequency (f_{max}) to prevent unwanted aliasing. The sampling rate condition is expressed as the inequality in [6]:

$$\text{Sampling rate condition: } f_s > 2f_{max} \qquad (7)$$

As shown in Figure 6, an amplified analog signal is brought from a charge amplifier and converted into a digitized signal, which is considered a digitized analog signal. However, a digitized analog signal is less likely to be effective because of its low sampling rate. To overcome this issue, the sampling time is set to decrease by switching the clock from 8 MHz to 72 MHz as the maximum clock (according to the datasheet of STM32, as shown in the table of the BOM). Thus, a dense digitized analog signal is formed owing to the higher sampling rate, which enables proper data processing for vibration analysis.

F. APPLICATION OF THE MATHEMATICAL EQUATIONS FOR THE MEASUREMENT OF VIBRATION

- Based on the formulation in [7], the magnitude of an analog voltage signal can be measured using the RMS, as the computation for data-sampled signals involves squaring the signal, averaging, and finally taking the square root. The expression for the RMS voltage (V_{RMS}) is shown below

$$V_{RMS} = \sqrt{\frac{1}{N}\sum_{i=1}^{N}[V(i)]^2} \qquad (8)$$

where N is the value of total sampled data count.

- To assess the piezoelectric sensor's role as an acceleration measurement device and the charge amplifier, which feeds raw voltage data to an STM32 to calculate RMS voltage, the relationship between the RMS voltage in V (from equation (8)) and voltage sensitivity in V/N (from equation (6)) is considered. The mass of a piezoelectric sensor (3 g) pressing tightly against an electrodynamic unit (141 g) is measured in kg ($= \frac{N}{ms^{-2}}$). The equation, derived from [4], for RMS acceleration in ms^{-2} can be expressed below

$$\text{RMS Acceleration}(ms^{-2}) = \frac{\text{RMS voltage (V)}}{\text{Sensitivity}\left(\frac{V}{N}\right) \text{ x mass (kg)}}$$

https://orcid.org/0009-0000-7509-6228

$$\text{RMS Acceleration}(\text{ms}^{-2}) = \frac{\text{RMS voltage (V)}}{8.51063 \text{ x } 10^{-2}(\frac{\text{V}}{\text{N}}) \text{ x } 0.144 \text{ (kg)}}$$

$$\text{RMS Acceleration}(\text{ms}^{-2}) = \frac{\text{RMS voltage (V)}}{8.51063 \text{ x } 10^{-2}(\frac{\text{V}}{\text{N}}) \text{ x } 0.144(\frac{\text{N}}{\text{ms}^{-2}})} \quad (9)$$

- The zero-crossing technique estimates the frequency of an oscillating signal by counting the number of times the waveform crosses the zero-amplitude point in a given amount of time. An easy and effective technique for evaluating the frequency of a regular sinusoidal wave without using FFT is to count the number of zero crossings. This approach recovers the so-called dominant frequency in signals composed of several sinusoidal components with changing magnitudes [8]. The equation for the frequency of a vibration signal using the zero-crossing method is given by

$$\text{f(Hz)} = \frac{\text{N}_{\text{zc}}}{2 \text{ x (SD)}} \quad (10)$$

where N_{zc} is the total number of zero-crossing events and SD represents the segment duration as the amount of time during which the zero crossings are counted.

G. MUTLIPLE TEMPERATURE SENSORS THROUGH THE ONE-WIRE PROTOCOL AND THE EQUATION FOR AN AVERAGE HEATING RATE

- The need to determine how long it actually takes to reach the target surface temperature, depending on the machinery's condition when a defect occurs. This equation, derived from [9], yields the average heating rate

$$= \frac{\text{(Target temperature} - \text{room temperature) in °C}}{\text{(heating time) in mins}} \quad (11)$$

where the room temperature is typically around 20 °C.

- In terms of using the one-wire protocol for multiple temperature sensors, temperature changes are detected by three digital temperature sensors (DS18B20) that instantly transmit their detected signals across the one-wire data bus without timing conflicts, and the STM32 microcontroller reads the data. Each digital temperature sensor has its own ROM, which the microcontroller scans to obtain separate output values for each sensor. The temperature range is between -55 °C and +125 °C (according to the datasheet, as indicated in the BOM table).

H. APPROPRIATE TEST SETUP FOR A FUNCTIONAL PROTOTYPE

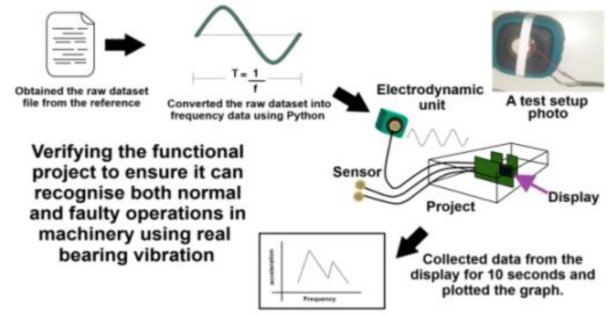

Figure 7. This illustrates how testing a prototype project using real machinery vibration signals actually worked. The raw bearing performance dataset was extracted from reference. An electrodynamic unit acted as a bearing with real bearing vibration.

Such methods are based on the testing technique illustrated in Figure 7.

- First, the raw datasets of both normal and defective bearing performance were extracted from the reference, which recorded them, and then converted into detectable vibration data using Python.

- Second, during the test setup, the center of the piezoelectric disc sensor was firmly pressed against an electrodynamic unit, which emits vibrations that a sensor detects. Instead of testing the machinery performance physically in a hazardous environment, this test setup is a safer technique to verify the project's functionality.

- Third, the recorded normal bearing vibration performance started running only for 10 seconds, allowing the piezoelectric disc sensor to detect vibration by converting physical mechanical motion into an electrical signal for measurements in Hertz and ms^{-2}. Again, another test for machinery's abnormal operation was conducted.

- Finally, once the data points for both normal and faulty bearing performance were collected from the project's display, the separated graphs were plotted for a careful survey.

III. COMPONENTS AND TOOLS USED

The bill of materials (BOM) is shown in the table below.

Main component name	Model name/ Part number	Specification	Description	Quantity	Purchase of date (based on receipts)	Datasheet reference
STM32 microcontroller	STM32F103	32-bit RISC, CPU, 72 MHz (maximum frequency).	A 32-bit microcontroller that performs tasks based on codes (C/C++ programming language).	1	October 2025	[10]
Piezoelectric disc sensor	ABT-441-RC	4200 Hz (resonant frequency), 20,000pF (capacitance),27 mm (brass), 20mm(ceramic)	Convert mechanical energy into an electrical signal using ceramics.	3	October 2025	[11]
Temperature sensor	DS18B20	+125 °C (maximum detected temperature).	Detect any thermal changes using the one-wire protocol.	3	October 2025	[12]
Operational amplifier	TL081	JFET input stage, 13–16 V/microsec (slew rate), 3-4 MHz (bandwidth).	The ability to amplify a weak signal depends on the external components.	3	October 2025	[13]
Organic light emitting diode (Display)	SSD1306	I2C protocol, small in size, and display.	Display real-time readings from the µC.	1	October 2025	[14]
ST-LINK debugger	ST-LINK/V2	JTAG/SWD (1.70V – 3.6V, 5 V as tolerant inputs).	Flash and update binary data into a microcontroller (STM32)	1	November 2025	-
Linear voltage regulator	LM7805	Input: 9V, Fixed 5V DC Output, 1.0A–1.5A max current.	Maintain a fixed 5V output.	1	January 2026	[15]

OLED (organic light-emitting diode) is an electronic display that shows real-time sensor readings from a DAQ system. It only supports half-duplex and short-distance communication. Real-time readings on the display are achieved by decreasing the sampling time while increasing the sampling rate, and the HAL delay is removed from the code, as it leads to a delayed response, to focus on managing time based on a clock signal. For proof of receipts, this paper has provided an ORCID link that has added GitHub carrying receipts for the main components. During development and verification, lab tools such as a soldering iron, a DMM, a voltmeter, and a variable power supply were used. A soldering iron was used to solder pads for electrical connections. A digital multi-meter (DMM) was utilized to measure the output voltage from a charge amplifier. A voltmeter was used to read the output voltage from a linear voltage regulator, such as LM7805, which is designed to maintain a fixed 5V output when the 9V battery is applied, to ensure that it would not affect the microcontroller (STM32F103), as it does not tolerate power beyond 5V as a tolerant power supply. Other lab equipment, such as a variable power supply, was used to power the entire circuit, which was testing the charge amplification board using a DMM for functional verification. An STM32 was being flashed using an ST-LINK debugger, which programmed the chip by loading the HAL-based code via advanced software (STM32CubeIDE).

https://orcid.org/0009-0000-7509-6228

IV. HARDWARE AND SOFTWARE IMPLEMENTATIONS

- HARDWARE IMPLEMENTATION

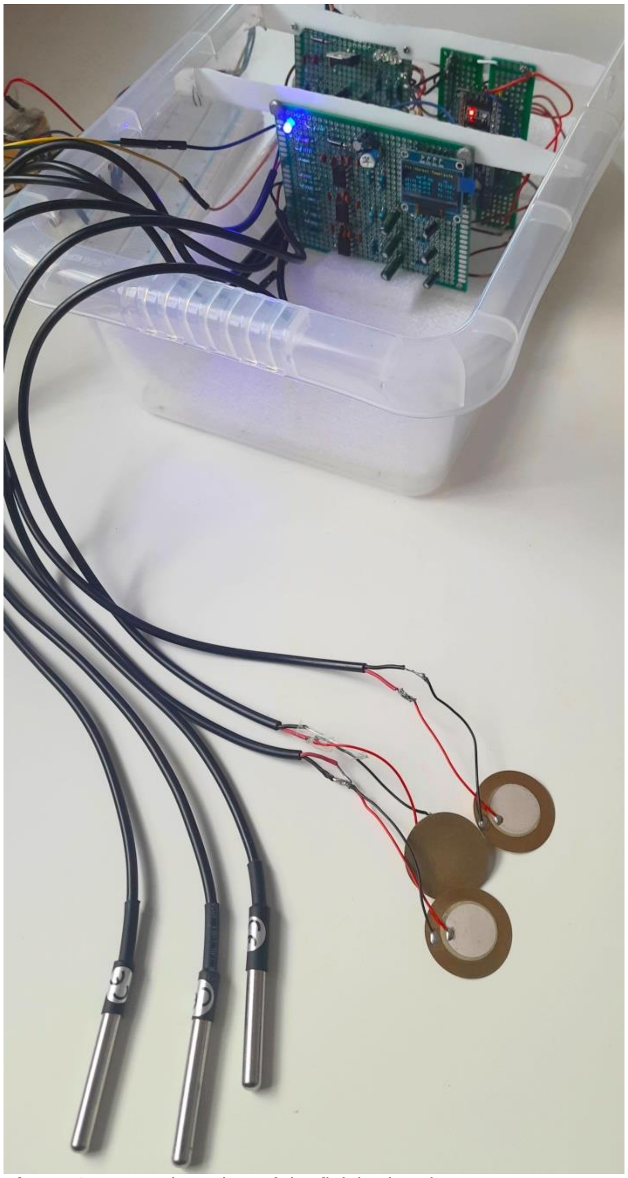

Figure 8. A complete view of the finished project.

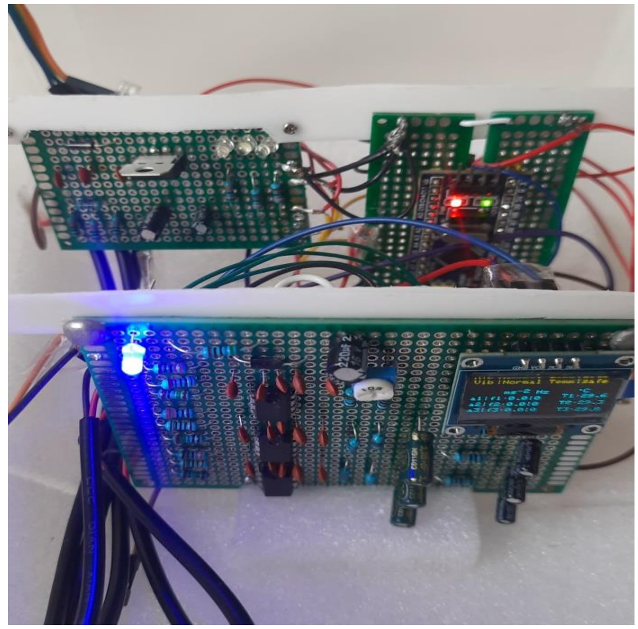

Figure 9. A close-up view of the finished project.

The hardware implementation has been completed. The front board in Figures 8 and 9 is the charge-amplification circuit, which was assembled by soldering. It holds the wires of three piezoelectric disc sensors for receiving raw analog inputs. The output terminals of the circuit are connected to the microcontroller board with red and green LEDs. The smaller board is a power supply board with a linear voltage regulator that provides a fixed 5V to the µC's 5V input pin. The same smaller board leaving some extra space holds the cables for three digital temperature sensors along with decoupling capacitors and other connections to the data acquisition system. Once detected, the signals are analyzed, and the results are displayed on the front board's screen for operators to view.

- SOFTWARE IMPLEMENTATION

The entire code for the STM32 is lengthy and is likely to be visible via GitHub. For this paper, it has been broken down into small sections of code for better comprehension. After processing mathematical calculations inside the data acquisition system, the output results are displayed on the SSD1306.

```
 int16_t readAnalogSignalfromchargeamp(uint32_t
channel)
{  /* read analog signal */
    ADC_ChannelConfTypeDef sConfig={0};
    sConfig.SamplingTime=
    ADC_SAMPLETIME_7CYCLES_5;
```

```
    sConfig.Channel = channel;
    sConfig.Rank= 1;
    HAL_ADC_ConfigChannel(&hadc1, &sConfig);
    HAL_ADC_Start(&hadc1);
    if (HAL_ADC_PollForConversion(&hadc1, 1) ==
    HAL_OK)
{
return HAL_ADC_GetValue(&hadc1);
}
Return 2048;
}
```

Figure 10. Enabling a setting to read each analog signal to determine vibration data in the STM32-based HAL code.

In terms of applying HAL-based codes via STM32CubeIDE for ADC, Figure 10 indicates that it permits STM32F103's ADC channels to read analog signals from the charge amplification circuit for data analysis. Note these codes are placed outside the main body.

```
while (1){
if (timenow - last_sample_time>= 1)
{
last_sample_time=timenow;
if (countingSample_N== 0)
{startingtime = timenow;}
uint16_t s1 =
readAnalogSignalfromchargeamp(ADC_CHANNEL_1);

uint16_t s2 =
readAnalogSignalfromchargeamp(ADC_CHANNEL_4);

uint16_t s3 =
readAnalogSignalfromchargeamp(ADC_CHANNEL_8);

float DigitizedAnalogsignal1 = (float)s1-
FilteroutALsignal1;

squaredvoltagesum1 +=
(DigitizedAnalogsignal1*DigitizedAnalogsignal1);
countingSample_N++;
}

if (countingSample_N >= 5) {

float insdEquat1 =
squaredvoltagesum1/(float)countingSample_N;

VoltageRMS1 = (sqrtf(insdEquat1)* Vrefereadc) /
Radc;

if (VoltageRMS1 < 0.04f)VoltageRMS1 = 0.0f;

squaredvoltagesum1 = 0.0f;
countingSample_N = 0;     }
}
```

Figure 11. Evaluating the RMS voltage 1 using a digitized analog signal from ADC channel 1. Similarly for RMS voltage 2 and RMS voltage 3 from ADC channels 4 and 8, respectively.

As shown in Figure 11, these programs in the main body are used to evaluate RMS voltage (from equation (8)) using a digitized analog signal from ADC channel 1 (A1 pin). Two more RMS voltages from ADC channel 4 (A2 pin) and ADC channel 8 (A3 pin) are being determined. Radc represents the resolution of the ADC, and Vrefereadc denotes the reference voltage (3.212V). During filtering, unwanted DC offsets are removed from the digitized analog signals of the three channels, converting them from unusable signals into measurable voltage signals.

```
if (timenow - last_sample_time>= 1)
 {
 last_sample_time=timenow;
 if (countingSample_N== 0)
 {
     startingtime = timenow;
 }
if ((DigitizedAnalogsignal1 >= 0.0f &&
lastAnalogsignal1 <
0.0f)||(DigitizedAnalogsignal1 < 0.0f &&
lastAnalogsignal1 >= 0.0f))
{
  NzcCount1 ++;
}
lastAnalogsignal1=DigitizedAnalogsignal1;
}
if (countingSample_N >= 5) {
float StartTimetoEndTime = 0.005f;

if (VoltageRMS1 < 0.04f)
{
  f1 = 0.0f ;
}
else
{
  f1 = ((float)  NzcCount1 /2.0f/
StartTimetoEndTime ;
}
Cleanedf1 =(f1*0.06f)+((0.52f+0.42f)*Cleanedf1);
NzcCount1 = 0.0f;
}
```

Figure 12. Calculating the zero-crossing rate for f1 using a digitized analog signal from ADC channel 1. Similarly for f2 and f3 from ADC channel 4 and ADC channel 8, respectively.

The codes in Figure 12 enable the determination of the zero-crossing rate using the total count of zero-crossing events. The calculation method is derived from equation (10) for the zero-crossing rate.

```
float Sensitivity = Q/Cf ;  /* Cf means feedback
capacitor*/

acceleration1 = VoltageRMS1/( Sensitivity *
mass); /* piezoelectric disc sensor as
accelerometer*/
```

Figure 13. Calculating the acceleration using RMS voltage 1 and voltage sensitivity. Similarly, for acceleration 2 and acceleration 3, using RMS voltages 2 and 3, respectively, with voltage sensitivity.

The codes in Figure 13 enable the calculation of

https://orcid.org/0009-0000-7509-6228

acceleration using RMS voltage and voltage sensitivity, as the acceleration is dependent on amplitude and magnitude. Such methods are derived from Equations (6), (8), and (9) for RMS-based acceleration.

```
DWT_Init();
DS18B20_ScanBus();
ssd1306_Init();
while (1)
{if (timenow-last_time_DS18B20_sensors>= 750){
last_time_DS18B20_sensors = timenow;
OneWire_Reset();
OneWire_WriteByte(0xCC);
OneWire_WriteByte(0x44);}
if (timenow-last_time_OLEDdisplay>= 250)
{
last_time_OLEDdisplay = timenow;
ssd1306_Fill(Black);
for (int i = 0; i < sensor_count; i++)
{float temp = DS18B20_Read(sensors[i].rom);
sprintf(handledata, "T%d:%.1f", i + 1, temp);
ssd1306_SetCursor(85, (i * 14) + 26);
ssd1306_WriteString(handledata, Font_6x8,
White);}
 ssd1306_UpdateScreen();
}
```

Figure 14. Reading DS18B20's unique ROM for a specific temperature sensor when it comes to having multiple sensors.

The codes used are shown in Figure 14 to enable reading each unique ROM of the temperature sensor (DS18B20) and scaling the temperature. All transmitted signals travel through a single wire called the One-Wire protocol, which should have zero timing conflicts. The temperature range measured by the sensor is only -55°C to +125°C. Once each temperature is detected, the results become visible on the display.

V. CHALLENGES

One minor challenge was an inevitable noise issue that kept showing up because of the lack of a ground plane, which is necessary to reduce noise during operation. Fortunately, the noise has been reduced using a software filter. Another minor challenge was that the STM32F103 package lacks a floating-point unit in its hardware specification, which limits the FFT (fast Fourier transform) processing for vibration analysis. In terms of obtaining the frequency domain, an alternative technique to FFT is the zero-crossing rate. However, this technique does not measure amplitude. Therefore, the acceleration can be calculated from the RMS voltage and sensitivity, as it is directly proportional to its amplitude. A major challenge during the development of this prototype was the hardware setup, as these dotted PCBs were difficult to manage due to many small wires soldered carefully to avoid short-circuit and open-circuit issues. Another major challenge was meticulously adjusting the microsecond timing on the one-wire protocol for industrial temperature sensors to ensure accurate operation.

VI. RESULTS AND DATA ANALYSIS

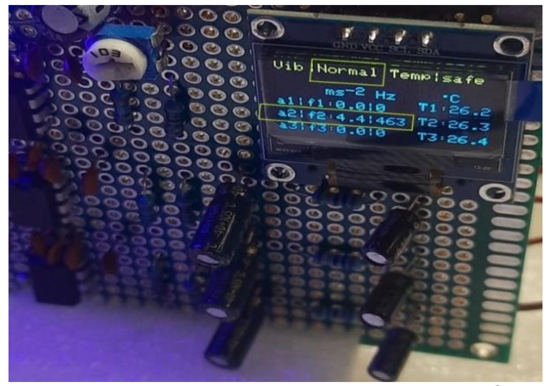

Figure 15. The detected vibration outputs (4.4 ms^{-2} at a frequency of 463 Hertz) are displayed, while the hardware prototype's sensor is capturing actual normal bearing vibration.

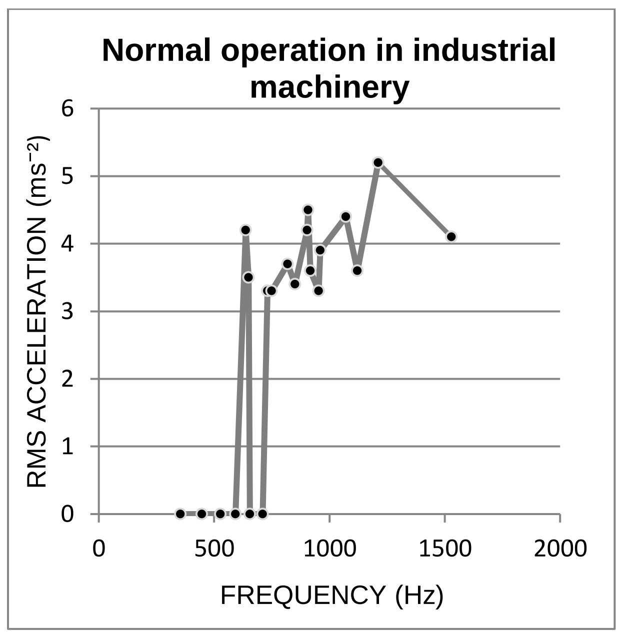

Figure 16. After collecting data points from the project's display during a 10-second normal bearing operation. The graph shows that the machinery is in normal condition, as all vibration values have reached below 6.5 ms^{-2} at the frequency ranges between 354 Hz and 1529 Hz.

In terms of obtaining real bearing vibration to verify the prototype's functionality, the raw datasets of both normal and abnormal bearing performance were

https://orcid.org/0009-0000-7509-6228

extracted from [16], which recorded them on Rexnord ZA-2115 double-row bearings during set part-one, and then translated into detectable vibration data using Python.

After using a hardware prototype to detect normal bearing vibration, this display in Figure 15 has received detected vibration signals as outputs (4.4 ms^{-2} and 463 Hertz). The status is showing normal, as the bearing is not unstable nor chaotic in motion. During testing, the actual sound is a hum and almost quiet. Based on the local visualization, no defect warning has appeared.

According to the previous experiment in [17], it has been confirmed that a possible sign of a bearing failure has been noticed when the vibration value exceeded 9 ms^{-2}.

These data points were collected from the electronic prototype's display during a 10-second normal bearing operation, while the sensor captured physical vibration at the same time. The plotted graph (see Figure 16) indicates that all data points have reached below 6.5 ms^{-2} at the frequency range between 354 Hz and 1529 Hz. For an industry standard (ISO 20816-3) in [18], it requires RMS vibration velocity values (in mm/s) to determine severity zones. Fortunately, the data points from the graph already include RMS acceleration and frequency. So, the RMS vibration velocity can easily be calculated as RMS acceleration divided by (2π x frequency) using these values (ms^{-2} and Hertz).

However, due to these different mathematical calculations this DAQ system processes, it does not strictly comply with ISO-20816-3, which also mandates a frequency limit of 1000 Hz [18]. But After converting to RMS vibration velocity using values (ms^{-2} and Hz) from the graph (see figure 16), most vibration velocity values, including 0.71 mm/s (calculated using 3.3 ms^{-2} at 732 Hz), 0.71 mm/s (calculated using 3.7 ms^{-2} at 819 Hz), 0.74 mm/s (calculated using 4.2 ms^{-2} at 903 Hz), 0.79 mm/s (calculated using 4.5 ms^{-2} at 907 Hz), 0.55 mm/s (calculated using 3.3 ms^{-2} at 953 Hz), 0.64 mm/s (calculated using 3.9 ms^{-2} at 960 Hz), accurately lie in the green zone (zone A). These mathematical conversions confirm that the vibration values fall precisely within the ISO-20816-3 severity zones. The collected data closely aligns with ISO 13373-1 guidelines, as shown in [19], regarding the use of RMS acceleration, while all normal-operation velocity vibration values are within the acceptable ISO 20816-3 severity threshold. Based on information from ISO 20816-3, if the vibration is increasing and the magnitude is projected not to exceed the upper limit of the normal range, no action is required, as machines with vibration magnitudes within the green zone are normally considered acceptable for unrestricted long-term operation.

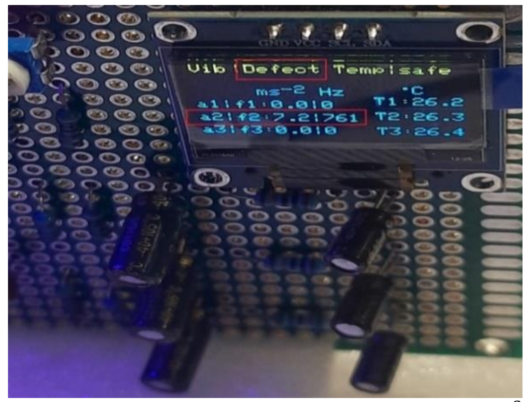

Figure 17. The detected vibration outputs (7.2 ms^{-2} at the frequency of 761 Hertz) are shown on the display with a defect warning status (shows up only when it reaches beyond 6.5 ms^{-2}), while the hardware prototype's sensor is capturing actual defective bearing vibration.

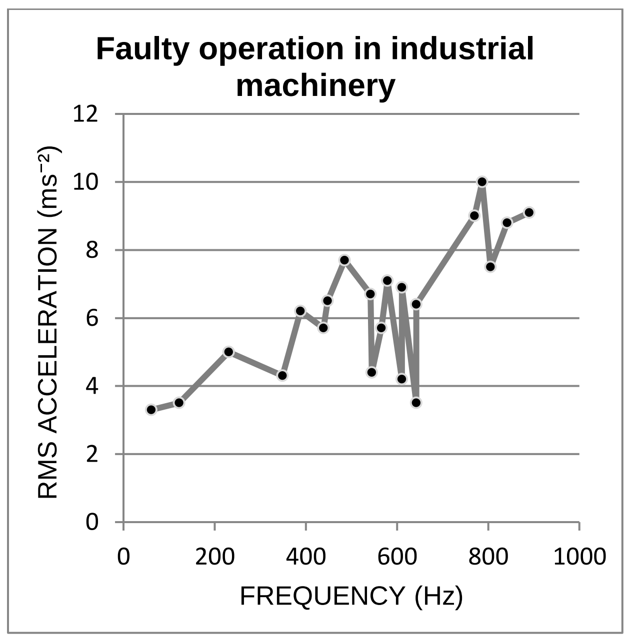

Figure 18. After collecting data points from the project's display during a 10-second defective bearing operation. The graph shows machinery is in an abnormal condition, as some vibration values have reached above 6.5 ms^{-2} at the frequency ranges between 448 Hz and 890 Hz.

After using a hardware prototype to detect defective bearing vibration, this display in Figure 17 has detected vibration signals as outputs ($7.2\ \mathrm{ms}^{-2}$ and 761 Hertz). During testing, the actual sound is unpleasantly loud, as the bearing is unstable and chaotic in motion. Based on the local visualization, a defect warning has appeared more frequently.

As shown in the graph above in Figure 18, some data points have reached above $6.5\ \mathrm{ms}^{-2}$ at the frequency range between 448 Hz and 890 Hz. One of the data points has reached $10\ \mathrm{ms}^{-2}$ at 787 Hz. After converting to RMS vibration velocity, some RMS vibration velocity values, including 2.31 mm/s (calculated using $6.5\ \mathrm{ms}^{-2}$ at 448 Hz) and 2.52 mm/s (calculated using $7.7\ \mathrm{ms}^{-2}$ at 485 Hz), lie in the yellow zone and are close to zone C. Some other velocity values, including 8.6 mm/s (calculated using $3.3\ \mathrm{ms}^{-2}$ at 61 Hz) and 3.4 mm/s (calculated using $5\ \mathrm{ms}^{-2}$at 231 Hz), fall in the red zone (zone D) and orange zone (zone C), respectively. Remember to note that this prototype does not strictly comply with ISO 20816-3, but some of these faulty-operation vibration values collected from the display accurately fall within the ISO 20816-3 severity zones, despite these different mathematical calculations processed by the DAQ system. Based on information from ISO 20816-3, if the vibration is increasing and the magnitude is projected to exceed the upper limit of the normal range. A more frequent monitoring schedule is needed, as machines with vibration magnitudes within zone C are normally considered unsatisfactory for long-term continuous operation. Zone D is generally considered dangerous, and the machine is required to shut down immediately only if vibration values remain in the red zone.

The testing footage for detecting normal and defective bearing operations can be shown through GitHub, which is added inside the ORCID link that this paper has given.

Apart from these graphs, the testing was conducted using empirical frame-by frame high speed video capture to closely analyze how long it took to display the result on the screen after creating a physical impact on a sensor. It has been verified that the end-to-end latency is 34 milliseconds, which is equivalent to 0.034 s, confirming the system has satisfied the criteria for real-time performance.

After a hands-on evaluation, in terms of estimating the average heating rate (from equation (11)) for the surface temperature of a motor (220-240V~50/60Hz, 400W, with protection), the target temperature is 38 °C (55 °C was expected to reach, but the surface temperature slowed down from increasing to 38 °C, as the motor is non-defective), the room temperature is 26 °C, and heating time is 11 mins. So the average heating rate is 1.09 °C per minute. This is considered a slow rate for the equivalent of healthy bearing temperature (around 40 °C, based on a previous survey in [17]). Moreover, this testing also indicates that the temperature reading accurately reflects the physical temperature. Hence, this functional prototype is suitable to use for monitoring an actual bearing's surface temperature.

Based on information in [20], the cost of an expensive 4-channel vibration monitoring device is typically around 4,000 EUR. This means a 1-channel device costs 1000 EUR. The 3-channel vibration monitoring device is still pricey, at about 3000 EUR.

This prototype project, which is also a 3-channel monitoring device involving both vibration and temperature sensors, is likely to cost approximately 60 EUR if it fits inside a medium-sized case, also depending on the total price of the components integrated into the PCBs. Therefore, the cost reduction is significant, at about 98 percent, after comparing the cost of a general 3-channel vibration monitoring device with that of this 3-channel project. It enables corporations to use this low-cost and real-time industrial monitoring device to gain an economic advantage.

VII. CONCLUSION

This electronic prototype has been verified, and it successfully recognizes both the normal and defective bearing operations in industrial machinery. As shown in the graph, after detecting faulty bearing vibration, some data points (including $6.5\ \mathrm{ms}^{-2}$ at 448 Hz and $7.7\ \mathrm{ms}^{-2}$ at 485 Hz), if converted into RMS vibration velocity values, jump into the yellow zone and are close to zone C. That is considered inadequate for long-term continuous operation. Whereas overall normal-operation vibration values remain within the green zone. Even with different mathematical techniques, the collected data from the display has confirmed this prototype's ability to monitor machinery health in close alignment with the principles of an industry standard, such as ISO 13373-1, while utilizing ISO 20816-3 severity zones to determine normal and abnormal operations. Following a hands-on evaluation, the temperature readings accurately reflect the physical surface temperature, enabling monitoring of

https://orcid.org/0009-0000-7509-6228

the surface temperature of an active physical bearing. Despite multiple sensors affecting performance speed, the response time delay is 34 milliseconds, equivalent to 0.034 s, confirming the system meets real-time monitoring criteria and visibly delivers faster performance. In addition to benefits, the cost reduction with this prototype is significant, at about 98%, after comparing it with the cost of a typical 3-channel monitoring device. This will allow corporations to use a low-cost and real-time industrial monitoring device that minimizes costs and maintenance efforts.

References

[1] A. Aherwar, "An investigation on gearbox fault detection using vibration analysis techniques: a review," 2012

[2] H. Elahi, A. Ali, H. Jabbar, A. B. Aqeel, A. Farrukh, S. Bibi, W. A. Altabey, S. A. Kouritem, and M. Noori, "Applications of piezoelectric-based sensors, actuators, and energy harvesters," 2025.

[3] Hui-fu Zhang , Wei Kang, "Design of the Data Acquisition System Based on STM32," 2013

[4] Mark Serridge, Torben R. Licht, "Piezoelectric Accelerometers and Vibration Preamplifiers handbook, " 1986

[5] Samuel E. Hall, Jaime E. Regis, Anabel Renteria, Luis A. Chavez, Luis Delfin, Sebastian Vargas, Michael R. Haberman, David Espalin, Ryan Wicker, Yirong Lin, "Paste Extrusion 3D Printing and Characterization of Lead Zirconate Titanate Piezoelectric Ceramics. " 2021

[6] J. Svatoš, J. Fischer, and J. Holub, "Increasing of Sampling Rate of Internal ADC in Microcontrollers by Equivalent-Time Sampling," in Proceedings of the 25th IMEKO TC4 International Symposium on Measurement of Electrical Quantities, Brescia, Italy, 2022, pp. 254-259, doi: 10.21014/tc4-2022.47.

[7] Moulin, "RMS Calculation for Energy Meter Applications Using the ADE7756," Analog Devices, Norwood, MA, USA, Application Note AN-578, 2001

[8] D. Yurin, M. Makukov, D. Kuvatova, A. Gluchshenko, and C. Omarov, "Applying zero-crossing method for frequency map analysis of dynamical systems, " 2024

[9] Y. Liang, S. Song, B. Xu, Z. Li, X. Li, Z. Mo, and J. Li, "Design of Small-Size Lithium-Battery-Based Electromagnetic Induction Heating Control System," 2024.

[10] "STM32F103x8 STM32F103xB datasheet, STMICROELECTRONICS." [Online]. Available: https://www.st.com/resource/en/datasheet/stm32f103c8.pdf

[11] "Piezo Element Datasheet: Piezoelectric Disc Sensors," Farnell, 2009. [Online]. Available: https://www.farnell.com/datasheets/360633.pdf

[12] "Programmable Resolution 1-Wire Digital Thermometer datasheet, DS18B20. " [Online]. Available: https://www.analog.com/media/en/technical-documentation/data-sheets/ds18b20.pdf

[13] "General purpose JFET single operational amplifiers datasheet, TL081, " [Online]. Available: https://www.st.com/resource/en/datasheet/tl081.pdf

[14] "SSD1306 datasheet, OLED (display), " [Online]. Available:https://cdn-shop.adafruit.com/datasheets/SSD1306.pdf

[15] "LM7805 Family datasheet, Texas Instruments, " [Online]. Available: https://www.ti.com/lit/ds/symlink/lm340.pdf

[16] Hai Qiu, Jay Lee, Jing Lin, IMS, university of Cincinnati. "Bearing Data Set", NASA Prognostics Data Repository, NASA Ames Research Center, Moffett Field, CA, 2007

[17] Wonho Jung, Sung-Hyun Yun, Yong-Hwa Park, "Vibration, and temperature run-to-failure dataset of ball bearing for prognostics, " 2024

[18] Mechanical vibration -Measurement and evaluation of machine vibration -Part 3. ISO 20816-3. 2022

[19] Condition monitoring and diagnostics of machines-Vibration condition monitoring -Part 1. ISO 13373-1. 2002

[20] A. Mystkowski, R. Kociszewski, A. Kotowski, M. Ciężkowski, W. Wojtkowski, M. Ostaszewski, Z. Kulesza, A. Wolniakowski, G. Kraszewski, and A. Idzkowski, "Design and Evaluation of Low-cost Vibration-Based Machine monitoring System For Hay Rotary Tedder, " 2022